

Λ and $\bar{\Lambda}$ Production in Central Pb-Pb Collisions at 40, 80, and 158 A·GeV

T. Anticic,²¹ B. Baatar,⁸ D. Barna,⁴ J. Bartke,⁶ M. Behler,¹³ L. Betev,⁹ H. Białkowska,¹⁹ A. Billmeier,⁹ C. Blume,⁷ B. Boimska,¹⁹ M. Botje,¹ J. Bracinik,³ R. Bramm,⁹ R. Brun,¹⁰ P. Bunčić,^{10,9} V. Cerny,³ P. Christakoglou,² O. Chvala,¹⁵ J.G. Cramer,¹⁷ P. Csátó,⁴ N. Dardenov,¹⁸ A. Dimitrov,¹⁸ P. Dinkelaker,⁹ V. Eckardt,¹⁴ P. Filip,¹⁴ D. Flierl,⁹ Z. Fodor,⁴ P. Foka,⁷ P. Freund,¹⁴ V. Friese,^{7,13} J. Gál,⁴ M. Gaździcki,⁹ G. Georgopoulos,² E. Gładysz,⁶ S. Hegyi,⁴ C. Höhne,¹³ K. Kadija,^{10,21} A. Karev,¹⁴ V.I. Kolesnikov,⁸ T. Kollegger,⁹ E. Kornas,⁶ R. Korus,¹² M. Kowalski,⁶ I. Kraus,⁷ M. Kreps,³ M. van Leeuwen,¹ P. Lévai,⁴ L. Litov,¹⁸ M. Makariev,¹⁸ A.I. Malakhov,⁸ C. Markert,⁷ M. Mateev,¹⁸ B.W. Mayes,¹¹ G.L. Melkumov,⁸ C. Meurer,⁹ A. Mischke,⁷ M. Mitrovski,⁹ J. Molnár,⁴ St. Mrówczyński,¹² G. Pál, ⁴ A.D. Panagiotou,² D. Panayotov,¹⁸ K. Perl,²⁰ A. Petridis,² M. Pikna,³ L. Pinsky,¹¹ F. Pühlhofer,¹³ J.G. Reid,¹⁷ R. Renfordt,⁹ W. Retyk,²⁰ C. Roland,⁵ G. Roland,⁵ M. Rybczyński,¹² A. Rybicki,⁶ A. Sandoval,⁷ H. Sann,⁷ N. Schmitz,¹⁴ P. Seyboth,¹⁴ F. Siklér,⁴ B. Sitar,³ E. Skrzypczak,²⁰ G. Stefanek,¹² R. Stock,⁹ H. Ströbele,⁹ T. Susa,²¹ I. Szentpétery,⁴ J. Sziklai,⁴ T.A. Trainor,¹⁷ D. Varga,⁴ M. Vassiliou,² G.I. Veres,⁴ G. Vesztergombi,⁴ D. Vranić,⁷ A. Wetzler,⁹ Z. Włodarczyk,¹² I.K. Yoo,¹⁶ J. Zaranek,⁹ and J. Zimányi⁴
(The NA49 Collaboration)

¹NIKHEF, Amsterdam, The Netherlands.

²Department of Physics, University of Athens, Athens, Greece.

³Comenius University, Bratislava, Slovakia.

⁴KFKI Research Institute for Particle and Nuclear Physics, Budapest, Hungary.

⁵MIT, Cambridge, USA.

⁶Institute of Nuclear Physics, Cracow, Poland.

⁷Gesellschaft für Schwerionenforschung (GSI), Darmstadt, Germany.

⁸Joint Institute for Nuclear Research, Dubna, Russia.

⁹Fachbereich Physik der Universität, Frankfurt, Germany.

¹⁰CERN, Geneva, Switzerland.

¹¹University of Houston, Houston, TX, USA.

¹²Institute of Physics Świętokrzyska Academy, Kielce, Poland.

¹³Fachbereich Physik der Universität, Marburg, Germany.

¹⁴Max-Planck-Institut für Physik, Munich, Germany.

¹⁵Institute of Particle and Nuclear Physics, Charles University, Prague, Czech Republic.

¹⁶Department of Physics, Pusan National University, Pusan, Republic of Korea.

¹⁷Nuclear Physics Laboratory, University of Washington, Seattle, WA, USA.

¹⁸Atomic Physics Department, Sofia University St. Kliment Ohridski, Sofia, Bulgaria.

¹⁹Institute for Nuclear Studies, Warsaw, Poland.

²⁰Institute for Experimental Physics, University of Warsaw, Warsaw, Poland.

²¹Rudjer Boskovic Institute, Zagreb, Croatia.

(Dated: November 9, 2018)

Production of Lambda and Antilambda hyperons was measured in central Pb-Pb collisions at 40, 80, and 158 A·GeV beam energy on a fixed target. Transverse mass spectra and rapidity distributions are given for all three energies. The Λ/π ratio at mid-rapidity and in full phase space shows a pronounced maximum between the highest AGS and 40 A·GeV SPS energies, whereas the $\bar{\Lambda}/\pi$ ratio exhibits a monotonic increase.

PACS numbers: 25.75.-q

Relativistic nucleus-nucleus collisions allow the investigation of hadronic matter at high temperatures and densities. One of the crucial features of nuclear collisions is the relative increase of strange particle production as compared to elementary hadron-hadron collisions. Systematic studies of hadron production in central A-A collisions have shown that this strangeness enhancement is not specific to the top SPS [1, 2] and RHIC [3, 4] energy range, $\sqrt{s_{NN}}$ from 18 to 200 GeV, but also occurs at the much lower AGS [5] and SIS [6] energies ($\sqrt{s_{NN}} < 6$ GeV). A theoretical view of the strangeness systematics was recently obtained when applying the Hagedorn

statistical hadronization model [7] in its grand canonical form. Contrary to the earlier analysis [8] which primarily focused on the energy density (assumed to be above the critical deconfinement phase transition energy density of about 1 GeV/fm³ predicted by lattice QCD [9]) the crucial parameter in the statistical model is the large coherent volume of the high density fireball [10] which is characteristic of central nucleus-nucleus collisions. The severe constraints of local strangeness conservation, characteristic of small volume elementary collisions, disappear, leading to an increase of the ratio of strange to non-strange hadron yields.

It was suggested [11] that the onset of deconfinement should cause a non-monotonic energy dependence of the total strangeness to pion ratio. This effect was recently observed in NA49 data on the energy dependence of kaon and pion production in central Pb-Pb collisions [12, 13] where a sharp maximum of the K^+/π^+ ratio is seen at 30 A·GeV beam energy ($\sqrt{s_{NN}} = 7.6$ GeV). To obtain an estimate of the energy dependence of total strangeness production and to study how the strange quarks and anti-strange quarks are distributed among the relevant hadronic species, it is important to complement the data of Refs. [12, 13] on K^+ and K^- yields by data on both Λ and $\bar{\Lambda}$ production.

In this letter we present measurements of Λ and $\bar{\Lambda}$ production in central Pb-Pb collisions at 40, 80, and 158 GeV per nucleon over a wide range in rapidity ($|y| \leq 1.6$, where y is the rapidity in the cms) and transverse mass m_T ($0 \leq (m_T - m_0) \leq 1.6$ GeV/ c^2 , where m_0 is the Λ mass). Preliminary analyses have been reported in Refs. [14, 15].

The NA49 detector is a large acceptance hadron spectrometer [16]. Tracking and particle identification by measuring the specific energy loss (dE/dx) is performed by two Time Projection Chambers (Vertex-TPCs), located inside two vertex magnets, and two large volume TPCs (Main-TPCs) situated downstream of the magnets symmetrically to the beam line. The relative dE/dx resolution is 4% and the momentum resolution $\sigma(p)/p^2 = 0.3 \cdot 10^{-4}$ (GeV/c) $^{-1}$. Centrality selection is based on a measurement of the energy deposited in a forward calorimeter by the projectile spectator nucleons. For the present analysis, the 7.2% most central interactions at 40 and 80 A·GeV were selected. Using the Glauber model to convert cross section fraction into number of wounded nucleons ($\langle N_W \rangle$) per event this corresponds, on average, to $\langle N_W \rangle = 349$ [12]. For 158 A·GeV the 10% most central events were selected ($\langle N_W \rangle = 335$). About 400 000 events were analyzed for 40 and 158 A·GeV each and 300 000 events for 80 A·GeV.

Λ and $\bar{\Lambda}$ hyperons are identified by reconstructing their decay topologies $\Lambda \rightarrow p + \pi^-$ and $\bar{\Lambda} \rightarrow \bar{p} + \pi^+$, respectively (branching ratio 63.9%). Candidates were found by forming pairs from all measured positively and negatively charged particles requiring a distance of closest approach between the two trajectories of less than 1 cm at any point before reaching the target plane. To reduce the combinatorial background from random pairs a set of quality cuts [17] was imposed on the position of the secondary vertex (at least 30 cm downstream from the target and outside the sensitive volume of the TPCs), on the impact parameter of the parent and the daughter tracks in the target plane, and on the number of points measured in the TPC. At 158 A·GeV an additional geometric quality cut was applied, which excludes particles in the high track density region from the analysis [17]. This results in a decreased acceptance for Λ and $\bar{\Lambda}$ at

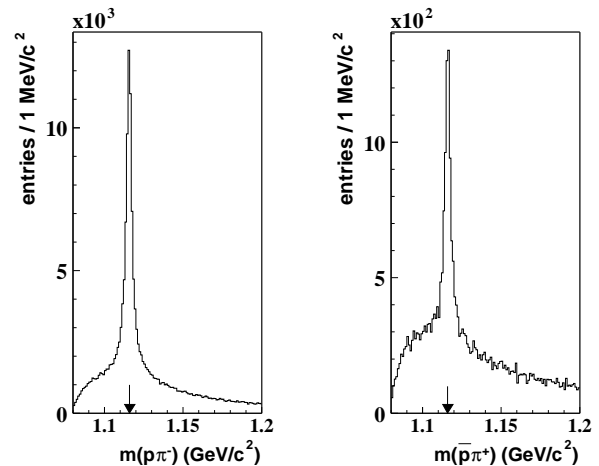


FIG. 1: Invariant mass distribution of Λ (left) and $\bar{\Lambda}$ (right) candidates in central Pb-Pb reactions at 158 GeV per nucleon. The Λ ($\bar{\Lambda}$) PDG mass (1.115 GeV/ c^2) is indicated by the arrows.

low transverse mass. For each Λ ($\bar{\Lambda}$) candidate the invariant mass was calculated assuming that the positive track is a proton (π^+) and the negative track is a π^- (\bar{p}). To enrich the decay protons (anti-protons) a cut on the specific energy loss dE/dx of the positive (negative) tracks of $\pm 4\sigma$ from the expected mean value was applied. In Fig. 1, the resulting invariant mass distributions of ($p\pi^-$) and ($\bar{p}\pi^+$) pairs at 158 A·GeV are shown. Clear signals are observed. The peak positions are in agreement with the nominal value of the Lambda hyperon mass [18]. The mass resolution (σ_m) is about 2 MeV/ c^2 at all three energies. The background was subtracted using a third-order polynomial. Corrections for geometrical acceptance, branching ratio and tracking efficiency were calculated bin by bin in rapidity and transverse momentum using GEANT 3.21 for detector simulation and dedicated NA49 simulation software [17]. The systematic errors were estimated by varying the quality cuts and by analyzing selected subvolumes of the TPCs and were found to be smaller than 9%. Corrections for feed-down from weak decays (mostly Ξ^- , Ξ^0 and their anti-particles) are not applied and were estimated to be less than 6% for Λ and less than 12% for $\bar{\Lambda}$. A detailed study shows a weak p_T and rapidity dependence. In the following Λ ($\bar{\Lambda}$) denotes also Λ ($\bar{\Lambda}$) from electro-magnetic Σ^0 ($\bar{\Sigma}^0$) decays.

The transverse mass distributions at mid-rapidity ($|y| \leq 0.4$) are shown in Fig. 2. All spectra are fitted by an exponential function in m_T :

$$\frac{1}{m_T} \frac{d^2n}{dm_T dy} \propto \exp\left(-\frac{m_T}{T}\right),$$

where T is the inverse slope parameter. The fitted range (in $m_T - m_0$) was 0.2–1.6 GeV/ c^2 for the Λ and 0.4–1.4 GeV/ c^2 for the $\bar{\Lambda}$. The results are summarized in Tab. I. The inverse slope parameter T increases with

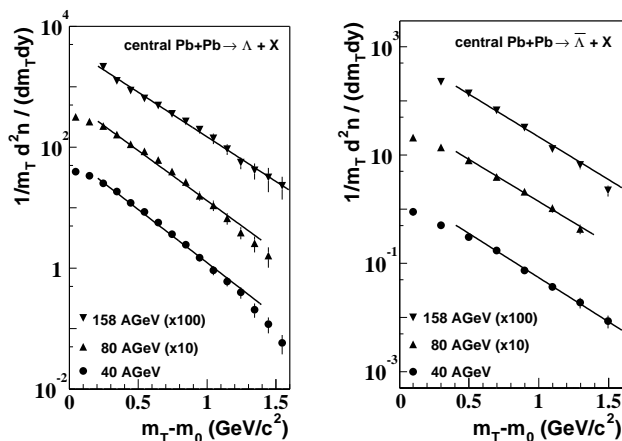


FIG. 2: Transverse mass spectra of Λ and $\bar{\Lambda}$ at mid-rapidity ($|y| \leq 0.4$). The full lines are exponential fits described in the text.

collision energy and is, within errors, the same for Λ and $\bar{\Lambda}$. The deviations at low transverse mass, seen in Fig. 2 for 40 and 80 A-GeV, and the convex shape of the spectra, indicate the effect of transverse flow [19].

Rapidity distributions are obtained by integrating the measured p_T spectra and by extrapolation into unmeasured regions. At 40 and 80 A-GeV the acceptance covers the full transverse momentum range down to $p_T = 0$. At 158 A-GeV the p_T integration was started at $p_T = 0.6$ GeV/c. The extrapolation to the full p_T range was performed by multiplying with factors 1.41 (Λ) and 1.35 ($\bar{\Lambda}$), which were derived from the 80 A-GeV p_T spectra. The resulting rapidity distributions of Λ and $\bar{\Lambda}$ hyperons are compared in Fig. 3. The Λ rapidity distribution at 40 A-GeV is peaked at mid-rapidity whereas this distribution becomes broader and flatter with increasing energy. Since Λ hyperons carry a significant fraction of the total net baryon number their rapidity distribution

	40A-GeV	80A-GeV	158A-GeV
$T(\Lambda)$ (MeV)	$247 \pm 10 \pm 20$	$272 \pm 11 \pm 22$	$295 \pm 13 \pm 23$
$T(\bar{\Lambda})$ (MeV)	$263 \pm 11 \pm 20$	$276 \pm 14 \pm 22$	$282 \pm 14 \pm 23$
dn/dy (Λ)	$15.3 \pm 0.6 \pm 1.0$	$13.5 \pm 0.7 \pm 1.0$	$10.9 \pm 1.0 \pm 1.3$
dn/dy ($\bar{\Lambda}$)	$0.42 \pm 0.04 \pm 0.04$	$1.06 \pm 0.08 \pm 0.1$	$1.62 \pm 0.16 \pm 0.2$
σ (Λ)	1.16 ± 0.06	-	-
σ ($\bar{\Lambda}$)	0.71 ± 0.05	0.85 ± 0.13	0.95 ± 0.05
$\langle \Lambda \rangle$	$45.6 \pm 1.9 \pm 3.4$	$47.4 \pm 2.8 \pm 3.5$	$44.1 \pm 3.2 \pm 5.0$
$\langle \bar{\Lambda} \rangle$	$0.74 \pm 0.04 \pm 0.06$	$2.26 \pm 0.25 \pm 0.2$	$3.87 \pm 0.18 \pm 0.4$

TABLE I: Inverse slope parameter T of the transverse mass spectra and the rapidity density dn/dy , both at mid-rapidity ($|y| \leq 0.4$), the width σ of the Gaussian fits to the rapidity distribution and the total multiplicity for Λ and $\bar{\Lambda}$ hyperons. The first error is statistical, the second systematic.

reflects the overall net baryon number distribution which is not peaked at mid-rapidity due to incomplete stopping of the incoming nucleons at top SPS energy. The same behaviour was observed for the y distribution of protons in central Pb-Pb collisions at this energy [20].

The Λ rapidity density at mid-rapidity (cf. Tab. I) decreases with increasing energy, whereas it increases for $\bar{\Lambda}$ hyperons. The inverse slope parameter and the mid-rapidity density at 158 A-GeV agree with previous data from WA97 [21]. The NA45 collaboration has measured Λ at 40 A-GeV [22]. Their extracted slope parameter is 25 MeV higher than the present result, but compatible within errors. Their mid-rapidity density ($dn/dy = 12 \pm 2$) also agrees within errors.

The total multiplicities are obtained by integrating the rapidity spectra with extrapolations into unmeasured regions using Gaussian fits for the $\bar{\Lambda}$ at all three energies and for the Λ at 40 A-GeV. A double Gaussian fit is used for the Λ at 80 A-GeV. For the Λ at 158 A-GeV an extrapolation is made using an average of the tails of the net-proton distribution at 158 A-GeV [20] and the Λ rapidity distribution in central S-S collisions [2]. The multiplicities in full phase space are summarized in Tab. I.

Remarkably, the Λ multiplicity shows no significant change between 40 and 160 A-GeV whereas $\bar{\Lambda}$ production grows by a factor of about 6. To compare these results with hyperon production in p-p collisions the yield is normalized to the mean pion multiplicity $\langle \pi \rangle = 1.5(\langle \pi^+ \rangle + \langle \pi^- \rangle)$, using measurements from NA49 [12] and E895 [23]. The energy dependence of the $\langle \Lambda \rangle / \langle \pi \rangle$ and $\langle \bar{\Lambda} \rangle / \langle \pi \rangle$ ratio is given as a function of collision energy $\sqrt{s_{NN}}$ in Figs. 4 and 5. The $\langle \Lambda \rangle / \langle \pi \rangle$ ratio steeply increases at AGS energies [24, 25] whereas it decreases

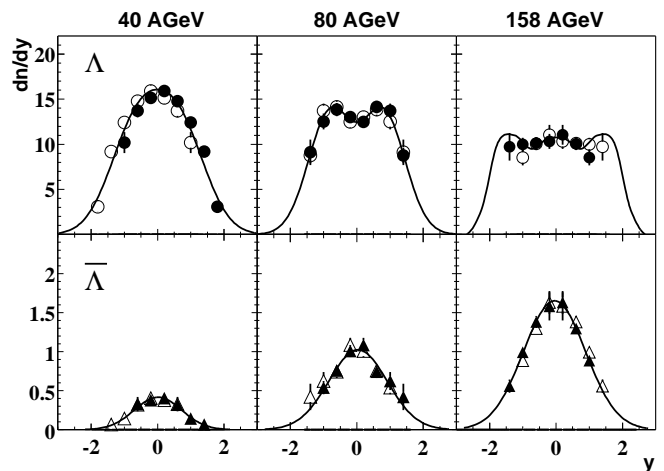


FIG. 3: Rapidity distribution of Λ (top) and $\bar{\Lambda}$ (bottom) at 40, 80, and 158 A-GeV beam energy (full symbols). The open symbols show the measured points, reflected with respect to $y = 0$. The errors are statistical only. The full lines represent fits to the data which were used to obtain total yields.

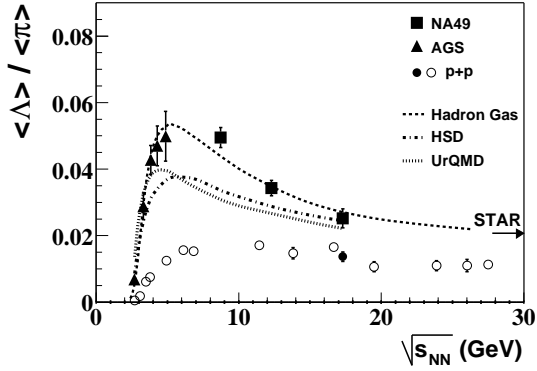


FIG. 4: The $\langle \Lambda \rangle / \langle \pi \rangle$ ratio in full phase space versus energy from NA49 (squares), AGS [24, 25] (triangles) and p-p reactions (Filled circle from NA49 and open circles from Refs. [27, 28]). The STAR measurements at mid-rapidity [26] are indicated by the arrow. The curves show predictions from the Hadron-gas model [30] (dashed), UrQMD [31] (dotted) and HSD [31] (dash-dotted).

gradually at SPS energies. The STAR measurement at $\sqrt{s_{NN}} = 130$ GeV [26] follows this trend. The $\langle \bar{\Lambda} \rangle / \langle \pi \rangle$ ratio, however, shows a monotonic increase up to RHIC energies [26] without significant structure. Qualitatively, the maximum in the $\langle \Lambda \rangle / \langle \pi \rangle$ ratio can be understood to arise from the interplay of the opening of the threshold of Λ -K associate production and the rapidly decreasing net baryon density in the produced fireball. In contrast, $\bar{\Lambda}$ production is not sensitive to the net baryon density and shows a continuous threshold increase.

For elementary p-p interactions [27, 28] the $\langle \Lambda \rangle / \langle \pi \rangle$ ratio shows an increase up to $\sqrt{s_{NN}} = 5$ GeV followed by a saturation at higher energies (cf. Fig. 4) with a similar trend observed in the $\langle \bar{\Lambda} \rangle / \langle \pi \rangle$ ratio (cf. Fig. 5). It is seen that both ratios are, at all energies, significantly below the A-A results. Consequently, Λ and $\bar{\Lambda}$ production in A-A collisions cannot be understood as a superposition of nucleon-nucleon interactions. The observed strangeness enhancement, both of $\langle \Lambda \rangle / \langle \pi \rangle$ and $\langle \bar{\Lambda} \rangle / \langle \pi \rangle$ in A-A collisions, is expected from the statistical hadronization model [10, 29, 30] which explains it as the fading-away of canonical strangeness suppression, characterizing the comparatively small fireball volume in p-p collisions.

Turning to the \sqrt{s} -dependence of strange to non-strange yield ratios we note, first, a close correspondence between the present Λ , $\bar{\Lambda}$ hyperon data and the K^+ , K^- data previously obtained by NA49 [12] for central Pb+Pb collisions at 40, 80 and 158 A-GeV. Both the $\langle \Lambda \rangle / \langle \pi \rangle$ and $\langle K^+ \rangle / \langle \pi \rangle$ ratios exhibit a distinct peak occurring between a steep rise toward top AGS energies, and a smooth fall-off from 40 A-GeV onward to RHIC energy. On the contrary both $\langle \bar{\Lambda} \rangle / \langle \pi \rangle$ and $\langle K^- \rangle / \langle \pi \rangle$ ascend monotonically toward RHIC energy. The latter yields are not affected

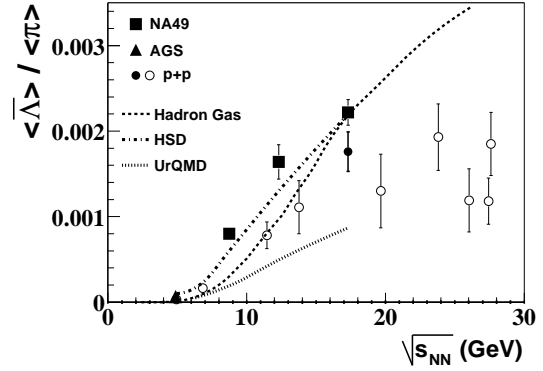


FIG. 5: The $\langle \bar{\Lambda} \rangle / \langle \pi \rangle$ ratio in full phase space versus energy from NA49 (squares), AGS [34] (triangles) and p-p reactions (Filled circle from NA49 and open circles from Refs. [27, 28]). The curves show predictions from the Hadron-gas model [30] (dashed), UrQMD [31] (dotted) and HSD [32, 33] (dash-dotted).

by the steep fall of the baryo-chemical potential. Since $\langle \Lambda \rangle \gg \langle \bar{\Lambda} \rangle$ and $\langle K^+ \rangle \gg \langle K^- \rangle$ in the interval from top AGS to low SPS energies, the Λ hyperons and K^+ carry a major fraction of the overall s and \bar{s} quark production. Thus $s + \bar{s}$ production, relative to $u + \bar{u} + d + \bar{d}$ production (as captured mostly in the pion yield) must reach a maximum within the interval $\sqrt{s} \approx 5$ GeV (top AGS energy) and $\sqrt{s} = 8.7$ GeV (the lowest SPS energy covered in the present study). As the corresponding p-p ratios vary much less over this energy range we finally conclude that the relative "strangeness enhancement" in A-A collisions reaches a maximum within this range.

The observed \sqrt{s} -dependence is confronted in Figs. 4 and 5 with predictions from the statistical hadronization ("hadron gas") model [30] and from the microscopic transport models UrQMD [31, 32] and HSD [31, 33]. The former employs a (T, μ_B) relation derived from a wide body of hadron production data [30] giving a reasonable overall account of $\langle \Lambda \rangle / \langle \pi \rangle$ and $\langle \bar{\Lambda} \rangle / \langle \pi \rangle$. The transport models also predict the main trend of the energy dependence, except the UrQMD model for the $\langle \bar{\Lambda} \rangle / \langle \pi \rangle$ ratio. Although model [31] describes well the lambda rapidity distributions, it fails for the ratios due to the overprediction of the pion multiplicities.

In summary, we have presented evidence for a relative strangeness enhancement maximum within the interval $5 \leq \sqrt{s} \leq 8$ GeV, as inferred both from the present hyperon data and from our previous kaon data [12]. Upcoming analysis of data gathered at the SPS inside this interval will decide as to whether the relatively smooth maximum implied by the (T, μ_B) relation assumed in the statistical hadronization model [30] captures the detailed features of that strangeness peak. First such K^+/π results obtained at $\sqrt{s} = 7$ GeV [13] seem to rather indicate a sharp peak as was

predicted for the onset of deconfinement, e.g. in Ref. [11].

Acknowledgements: This work was supported by the US Department of Energy Grant DE-FG03-97/ER41020/A000, the Bundesministerium für Bildung und Forschung, Germany, the Polish State Committee for Scientific Research (2 P03B 130 23, SPB/CERN/P-03/Dz 446/2002-2004, 2 P03B 02418, 2 P03B 04123), the Hungarian Scientific Research Foundation (T032648, T043514 and T32293), Hungarian National Science Foundation, OTKA, (F034707), and the Polish-German Foundation.

-
- [1] J. Bartke *et al.*, Z. Phys. **C48**, 191 (1990).
 - [2] T. Alber *et al.*, Z. Phys. **C64**, 195 (1994).
 - [3] C. Adler *et al.*, nucl-ex/0206008.
 - [4] K. Adcox *et al.*, Phys. Rev. Lett. **88**, 242301 (2002).
 - [5] L. Ahle *et al.*, Phys. Rev. **C60**, 044904 (1999).
 - [6] J. Cleymans, H. Oeschler, and K. Redlich, Phys. Lett. **B485**, 27 (2000).
 - [7] R. Hagedorn, Nucl. Phys. **B24**, 93 (1970).
 - [8] J. Rafelski and B. Müller, Phys. Rev. Lett. **48**, 1066 (1982).
 - [9] F. Karsch, Nucl. Phys. **A698**, 199c (2002).
 - [10] A. Tounsi and K. Redlich, J. Phys. G **28**, 2095 (2002).
 - [11] M. Gaździcki and M. Gorenstein, Acta Phys. Polon. **B30**, 2705 (1999).
 - [12] S.V. Afanasiev *et al.*, Phys. Rev. **C66**, 054902 (2002).
 - [13] V. Friese *et al.*, nucl-ex/0305017.
 - [14] A. Mischke *et al.*, J. Phys. G **28**, 1761 (2002).
 - [15] A. Mischke *et al.*, Nucl. Phys. **A715**, 453c (2003).
 - [16] S.V. Afanasiev *et al.*, Nucl. Instrum. Meth. **A430**, 210 (1999).
 - [17] A. Mischke, Ph.D. thesis, University of Frankfurt (2002).
 - [18] K. Hagiwara *et al.* (Particle Data Group), Phys. Rev. **D66**, 010001 (2002).
 - [19] E. Schnedermann, J. Sollfrank, and U. Heinz, Phys. Rev. **C48**, 2462 (1993).
 - [20] H. Appelshäuser *et al.*, Phys. Rev. Lett. **82**, 2471 (1999).
 - [21] F. Antinori *et al.*, Nucl. Phys. **A661**, 130c (1999).
 - [22] W. Schmitz *et al.*, J. Phys. G **28**, 1861 (2002).
 - [23] J.L. Klay *et al.*, nucl-ex/0306033, accepted by Phys. Rev. C.
 - [24] C. Pinkenburg *et al.*, Nucl. Phys. **A698**, 495c (2002).
 - [25] F. Becattini *et al.*, Phys. Rev. **C64**, 024901 (2001).
 - [26] C. Adler *et al.*, Phys. Rev. Lett. **89**, 092301 (2002).
 - [27] M. Gaździcki and D. Röhrich, Z. Phys. **C71**, 55 (1996).
 - [28] M. Gaździcki and D. Röhrich, Z. Phys. **C65**, 215 (1995).
 - [29] A. Tounsi, A. Mischke, and K. Redlich, Nucl. Phys. **A715**, 565c (2003).
 - [30] P. Braun-Munzinger, J. Cleymans, H. Oeschler, and K. Redlich, Nucl. Phys. **A697**, 902 (2002), and private communication.
 - [31] H. Weber, E.L. Bratkovskaya, W. Cassing, and H. Stöcker, Phys. Rev. **C67**, 014904 (2003).
 - [32] H. Weber, E.L. Bratkovskaya, and H. Stöcker, nucl-th/0205032, and private communication.
 - [33] W. Cassing, Nucl. Phys. **A700**, 618 (2002).
 - [34] B.B. Back *et al.*, Phys. Rev. Lett. **87**, 242301 (2001).